

Cite this: *Chem. Sci.*, 2023, **14**, 4769

All publication charges for this article have been paid for by the Royal Society of Chemistry

Received 13th February 2023

Accepted 30th March 2023

DOI: 10.1039/d3sc00806a

rsc.li/chemical-science

Snapshots of sequential polyphosphide rearrangement upon metallatetraylene addition^{†,‡}

Xiaofei Sun, ^a Alexander Hinz, ^a Stephan Schulz, ^b Lisa Zimmermann, ^c Manfred Scheer ^c and Peter W. Roesky ^{*a}

Insertion and functionalization of gallasilylenes $[L^{Ph}Si-Ga(Cl)L^{BDI}]$ ($L^{Ph} = PhC(NtBu)_2$; $L^{BDI} = \{[2,6-iPr_2C_6H_3NCMe_2CH]\}$) into the *cyclo-E₅* rings of $[Cp^*Fe(\eta^5-E_5)]$ ($Cp^* = \eta^5-C_5Me_5$; $E = P, As$) are reported. Reactions of $[Cp^*Fe(\eta^5-E_5)]$ with gallasilylene result in $E-E/Si-Ga$ bond cleavage and the insertion of the silylene in the *cyclo-E₅* rings. $\{[L^{Ph}Si-Ga(Cl)L^{BDI}](\eta^4-P_5)FeCp^*\}$, in which the Si atom binds to the bent *cyclo-P₅* ring, was identified as a reaction intermediate. The ring-expansion products are stable at room temperature, while isomerization occurred at higher temperature, and the silylene moiety further migrates to the Fe atom, forming the corresponding ring-construction isomers. Furthermore, reaction of $[Cp^*Fe(\eta^5-As_5)]$ with the heavier gallagermylene $[L^{Ph}Ge-Ga(Cl)L^{BDI}]$ was also investigated. All the isolated complexes represent rare examples of mixed group 13/14 iron polypnictogenides, which could only be synthesized by taking advantage of the cooperativity of the gallatetraylenes featuring low-valent Si(II) or Ge(II) and Lewis acidic Ga(III) units/entities.

Introduction

Cooperativity between two metals has offered significant opportunities in the areas of bond activation and catalysis.¹ Bimetallic complexes often show unique transformation pathways which is ascribed to the synergy between the two elements, such reactions are difficult to achieve using a monometallic reagent. Cooperative effects may not only occur if a metal–metal bond is present but also if the two metal centers are in close spatial proximity. During recent decades, a great variety of homo- and heterobimetallic transition-metal species were developed that enable extraordinary chemical transformations.² Not only for transition-metals but also when main group elements participate, cooperative effects are observed. Well established systems are for example frustrated Lewis pairs (FLPs)³ or mixed alkali metal/main group element systems.^{4a,4} As for homobinuclear low-valent main group systems, Driess' bis(silylenes)⁵ and Jones' Mg(I) dimers⁶ are for example well-developed compounds, showing unexpected chemical transformations owing to the synergy created between the two

low-valent elements. Very recently, the synthesis of metallatetraylene systems which combine a low-valent tetraylene site and a Lewis acidic group 13 metal functionalization has been reported.⁷ Initial reactions with white phosphorus (P_4) resulted in unprecedented $[2 + 1 + 1]$ fragmentations of the P_4 tetrahedron and formation of rare mixed group 13/14 phosphorus chain species.^{7a} Those transformation and fragmentation reactions of P_4 are unique and cannot be obtained using classical mono-tetraylenes.⁸ Such heterometallic group 13/14 systems provided new avenues for cooperative transformations which are worth exploring reagents in the area of polypnictogenide chemistry.

Since the pioneering synthesis of the air-stable pentaphosphaphaferrocene $[Cp^*Fe(\eta^5-P_5)]$ by Scherer,⁹ it has been used as a well-established building block in coordination¹⁰ and supramolecular chemistry.¹¹ The reactivity has been investigated extensively with reactive transition metal complexes,¹² and with highly reducing lanthanide compounds.¹³ Redox reactions with $[Cp^*Fe(\eta^5-P_5)]$ often involve the *cyclo-P₅* moiety without alteration of the ring itself. The reactivity towards a low-valent p-block compound was discovered recently (Scheme 1), this can be accompanied by selective substitution and insertion reactions.¹⁴ For example, when using Si(I) or Si(II) species, selective insertion and substitution reactions of the *cyclo-P₅* moiety are observed, leading to unusual $[4 + 1]$ fragmentation (*cyclo-SiP₄-SiP*) or Si-P substitution (*cyclo-SiP₄*) ring products (Scheme 1a).¹⁵ Using different Al(I) nucleophiles, either an Al-functionalized bent *cyclo-P₅* moiety or a cage-type structural motif was observed, the latter one was formed by $[4 + 1]$ fragmentation (Scheme 1a).¹⁶ Molecular main group polypnictogenides are indeed an interesting class of compounds

^aInstitute of Inorganic Chemistry, Karlsruhe Institute of Technology (KIT), Engesserstraße 15, Karlsruhe, 76131, Germany. E-mail: roesky@kit.edu

^bInstitute for Inorganic Chemistry and Center for Nanointegration Duisburg-Essen (Cenide), University of Duisburg-Essen, Universitätsstraße 5–7, Essen, 45117, Germany

^cInstitute of Inorganic Chemistry, University of Regensburg, Universitätsstr. 31, Regensburg 93040, Germany

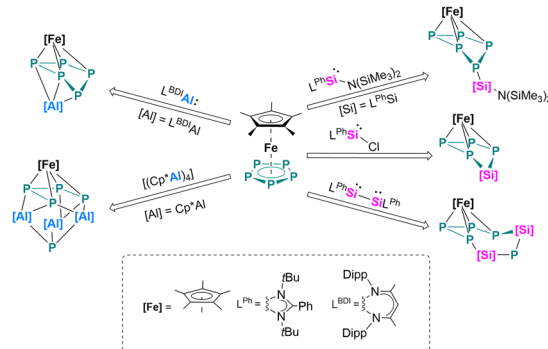
† Dedicated to Professor Hongjian Sun on the occasion of his 60th birthday.

‡ Electronic supplementary information (ESI) available. CCDC 2225385–2225391.

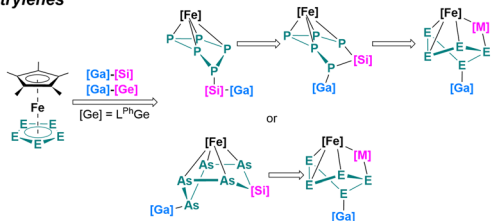
For ESI and crystallographic data in CIF or other electronic format see DOI: <https://doi.org/10.1039/d3sc00806a>



(a) Previous work: Reactivity toward low-valent mononuclear p-block species



(b) This work: Cooperative transformation by binuclear mixed group 13/14 tetrylenes



Scheme 1 (a) Previous work: Reactivity of $[\text{Cp}^*\text{Fe}(\eta^5\text{-P}_5)]$ towards low-valent p-block species;^{15,16} (b) overview of this work.

with growing interests. However, the reactivity of $[\text{Cp}^*\text{Fe}(\eta^5\text{-E}_5)]$ ($\text{E} = \text{P, As}$) with low-valent p-block compounds is still limited,^{14–17} and most of the examples only utilizing monometallic/mononuclear reagents.

In this work, the cooperativity of heterobimetallic gallate-tetrylenes is showcased by selective coordination, and insertion in the iron-coordinated polypnictogenes $[\text{Cp}^*\text{Fe}(\eta^5\text{-E}_5)]$ ($\text{E} = \text{P, As}$). By controlling the reaction temperature, a consecutive isomerization pathway took place, enabling to identify different isomers, representing first examples of mixed group 13/14 polypnictogenides.

Results and discussion

The reaction of equimolar amounts of $[\text{Cp}^*\text{Fe}(\eta^5\text{-P}_5)]$ and $[\text{L}^{\text{Ph}}\text{Si}-\text{Ga}(\text{Cl})\text{L}^{\text{BDI}}]$ [$\text{L}^{\text{Ph}} = \text{PhC}(\text{NtBu})_2$; $\text{L}^{\text{BDI}} = \{[\text{2,6-iPr}_2\text{C}_6\text{H}_3-\text{NCMe}\}_2\text{CH}$] at room temperature immediately resulted in

a dark red reaction mixture (Scheme 2). Monitoring the reaction under these conditions by $^{31}\text{P}\{^1\text{H}\}$ NMR spectroscopy revealed the formation of two sets of $^{31}\text{P}\{^1\text{H}\}$ NMR patterns, indicative of two different products. The minor component **1** shows one broad featureless resonance at 57.0 ppm, and the major species **2** shows an AMXYZ spin system, with five signals at 86.0, 44.8, 28.7, -3.6, -219.2 ppm, and large P-P coupling constants (314–414 Hz) pointed to a classical polyphosphide structure. In solution, the signals of the minor product **1** decreased rapidly and within about 30 min, the dark red solution turned brown and only the major product **2** is visible, indicating an isomerization from **1** to **2**. Crystallization from *n*-hexane gave orange prisms of the reaction product **2** in 41% yield. The results of the single crystal diffraction measurements reveal an insertion of the $[\text{L}^{\text{Ph}}\text{Si}]$ moiety into the P_5 -ring of $[\text{Cp}^*\text{Fe}(\eta^5\text{-P}_5)]$. Complex **2** thus consists of a unique six-membered silapentaphospho-ring with one of the phosphorus atoms P1 additionally coordinated by the $[\text{L}^{\text{BDI}}\text{GaCl}]$ fragment (Fig. 1). In this reaction, the Ga-Si bond is cleaved and subsequently, complex **2** is formed through insertion of the silylene $[\text{L}^{\text{Ph}}\text{Si}]$ moiety into one P-P bond. In the polyphosphide moiety, the $[\text{Cp}^*\text{Fe}]^+$ unit is η^4 -coordinated to

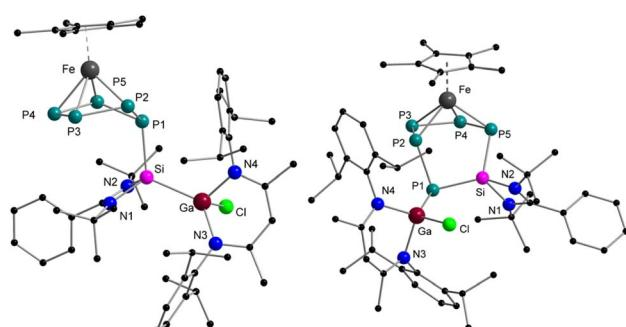
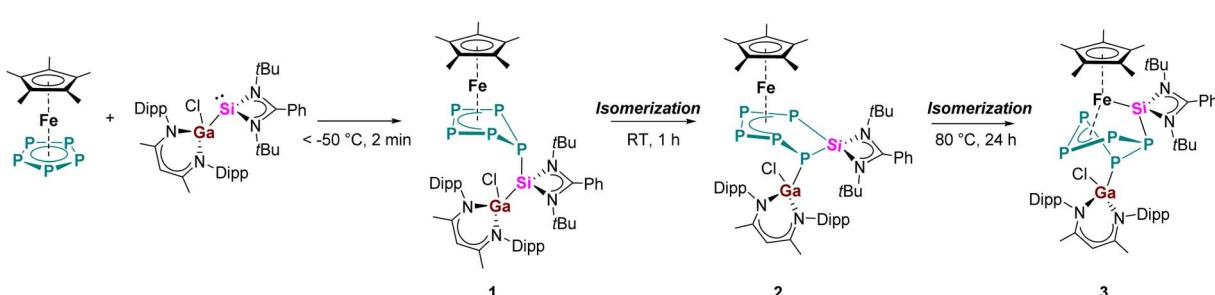


Fig. 1 Molecular structures of complexes **1** (left) and **2** (right) in the solid state. Selected bond distances [Å] and angles [°] in **1**: Ga–Si 2.4293(11), P1–P2 2.1583(15), P2–P3 2.148(2), P3–P4 2.133(2), P4–P5 2.145(2), P1–P5 2.1682(14), P1–Si 2.2516(14), Fe–P2 2.3096(12), Fe–P3 2.3305(13), Fe–P4 2.3245(13), Fe–P5 2.3063(12); P1–P2–P3 109.04(6), P2–P3–P4 103.87(6), P3–P4–P5 104.41(7), P4–P5–P1 108.56(6), P2–P1–P5 94.68(6). In **2**: P1–P2 2.2403(9), P2–P3 2.1467(10), P3–P4 2.1619(10), P4–P5 2.1565(10), Si–P1 2.1771(9), Si–P5 2.1985(9), Ga–P1 2.3062(7), Fe–P2 2.2653(7), Fe–P3 2.3266(8), Fe–P4 2.3471(7), Fe–P5 2.2595(7); P1–P2–P3 100.56(4), P2–P3–P4 105.26(4), P3–P4–P5 108.18(4), P4–P5–Si 106.33(4), P1–Si–P5 113.40(4), Si–P1–P2 95.90(3).



Scheme 2 Reactivity of pentaphosphaferrocene $[\text{Cp}^*\text{Fe}(\eta^5\text{-P}_5)]$ towards gallasilylene $[\text{L}^{\text{Ph}}\text{Si}-\text{Ga}(\text{Cl})\text{L}^{\text{BDI}}]$.



P2–P5 and within this moiety, all P–P bond lengths (P2–P3 2.1467(10) Å, P3–P4 2.1619(10) Å, P4–P5 2.1565(10) Å) are between P–P single and double bonds.¹⁸ In contrast, the longer P1–P2 bond of 2.2403(9) Å indicates a classical single bond. The Si–P1 (2.1771(9) Å) and Si–P5 (2.1985(9) Å) bond distances are between the reported distances of Si–P single (2.24–2.27 Å) and double bonds (2.06–2.09 Å).^{8c,18} Moreover, the Ga–P1 bond length (2.3062(7) Å) agrees with the Ga–P single bonds found in $[L^{BDI}Ga(O_3SCF_3)(PPh_2)]$ (2.312(3) Å)¹⁹ and is considerably longer than in the gallaphosphene $[L^{BDI}(Cl)GaPGaL^{BDI}]$ (2.1613(6) Å, 2.2688(5) Å).²⁰ The 1H NMR spectrum shows four sets of $CH(CH_3)_2$ signals of the iPr groups in the L^{BDI} ligand pointing to their inequivalency in solution due to restricted rotation. Similarly, two distinct singlets of the *t*Bu groups were found at 0.74 and 1.37 ppm, respectively. The $^{29}Si\{^1H\}$ NMR spectrum exhibited a single resonance at 57.1 ppm, which is slightly upfield shifted compared to the gallasilylene (65.1 ppm). The reactivity observed in this case is different from the previously known reactions of pentaphosphoferrocene $[Cp^*Fe(\eta^5-P_5)]$ (Scheme 1), as a ring expansion occurred without fragmentation of the P_5 moiety. This selective insertion of the silylene into P–P bond which led to ring expansion and P-functionalization reaction is indeed unprecedented, compared to the chlorosilylene $[L^{Ph}SiCl]$, which gave the substitution product and thus forming a tetraphosphasila-five-membered heterocycle. The effect of the Ga-functionalization in the silylene is crucial, since the additional Lewis-acidic center associates the redox-reaction process.

Now that the molecular structure of the reaction product 2 has been established, the identity of the short-lived intermediate 1 still had to be elucidated. Therefore, an NMR-scale experiment between the two starting materials $[Cp^*Fe(\eta^5-P_5)]$ and $[L^{Ph}Si-Ga(Cl)L^{BDI}]$ at low temperatures was carried out. In order to prevent the fast isomerization from 1 to 2, toluene- d_8 was condensed into a J. Young NMR tube containing solid mixture of two starting materials at $-196^{\circ}C$. The mixture was carefully warmed up to $-80^{\circ}C$ and a $^{31}P\{^1H\}$ NMR spectrum was taken immediately at this temperature (Fig. 2). The $^{31}P\{^1H\}$ NMR spectrum of 1 reveals three sets of multiplets for the five P atoms, an apparent AA'MM'X spin system, which is typical for envelope-shaped *cyclo-P₅* rings.^{13b,c,14,15,21} Simulations of the $^{31}P\{^1H\}$ NMR spectra were performed using gNMR simulation software²² by an iterative fitting process (Fig. 2 and see ESI, S21†). Since $[L^{Ph}Si-N(SiMe_3)_2]$ forms with $[Cp^*Fe(\eta^5-P_5)]$ the P–Si adduct $\{[L^{Ph}Si-N(SiMe_3)_2]\}(\eta^4-P_5)FeCp^*$ (Scheme 1a),¹⁵ we anticipated that in the present investigation the strong nucleophilic divalent silicon center of $[L^{Ph}Si-Ga(Cl)L^{BDI}]$ attacks the P_5 -ring of $[Cp^*Fe(\eta^5-P_5)]$ in the first step and coordinates towards one P atom (see below for DFT calculations).

This hypothesis was unambiguously corroborated by single crystal X-ray diffraction analysis. During NMR experiments, compound 1 could be crystallized as red prism, which then decomposes within a few min in solution. The molecular structure of 1 is depicted in Fig. 1 and as proposed by the ^{31}P NMR results, the *cyclo-P₅* unit reveals a bent envelope-shaped conformation with P1 deviating out of the plane. The bonding metrics in the polyphosphide moiety is comparable to that in

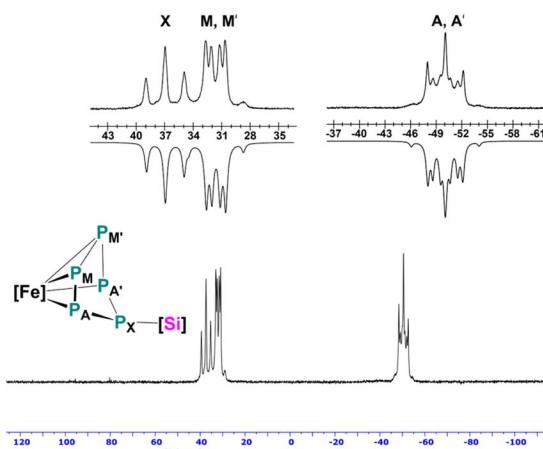


Fig. 2 $^{31}P\{^1H\}$ NMR spectrum at 193 K of 1 measured in $tol-d_8$ with nuclei assigned to an AA'MM'X spin system; insets: extended signals (upward) and simulations (downward); $[Fe] = Cp^*Fe$; $[Si] = L^{Ph}Si-Ga(Cl)L^{BDI}$.

$\{[L^{Ph}Si-N(SiMe_3)_2]\}(\eta^4-P_5)FeCp^*$.¹⁵ Further reaction of 1 was monitored by $^{31}P\{^1H\}$ -VT NMR studies (see ESI, Fig. S1†) and while increasing the temperature, the signals of 1 become broader and already at $-10^{\circ}C$, small amounts of the isomerization product 2 are visible.

Furthermore, we noticed that even compound 2 is stable at room temperature both in solid state and in C_6D_6 , it slowly decomposes at higher temperatures. When a solution of 2 was heated for more than 24 h to $80^{\circ}C$, all signals belonging to 2 disappeared and a new set of signals appeared (224.8, 89.3, 12.8, -56.8 , -66.8 ppm), exhibiting an AMNZX spin system character. Crystallization from C_6D_6 led to the isolation of green-colored prisms, which could be identified by single crystal X-ray diffraction analysis (Scheme 1 and Fig. 3). The isolated complex 3 is the thermodynamically most favored isomer of complexes 1 and 2 which is formed by P1–P5 bond formation along with the P1–Si1 bond cleavage. Thus, in this step the P_5Si ring in 2, contracts back to a bent P_5 ring. The $[L^{Ph}Si]^+$ moiety migrates along the polyphosphide moiety to the iron atom, and

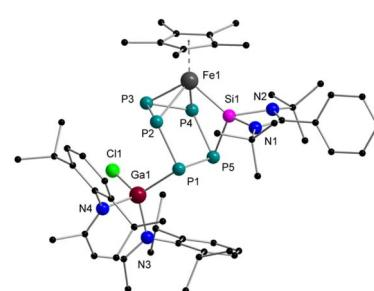


Fig. 3 Molecular structure of complex 3 in the solid state. Selected bond distances [Å] and angles [°]: Ga1–Cl1 2.2108(11), Ga1–P1 2.3117(12), Fe1–Si1 2.2081(14), Si1–P5 2.255(2), P1–P2 2.218(2), P2–P3 2.149(2), P3–P4 2.111(2), P4–P5 2.318(2), P1–P5 2.187(2), P2–P1–P5 101.74(5), P1–P2–P3 103.72(7), P2–P3–P4 99.07(7), P3–P4–P5 107.78(6), P4–P5–P1 102.12(6).



further inserts into an Fe–P bond, resulting in an unusual η^3 -coordination mode of the P_5 ring to the $[\text{Cp}^*\text{Fe}]^+$ moiety. One of the phosphorus atoms (P1) is further functionalized by the gallarylene moiety $[\text{L}^{\text{BDI}}\text{GaCl}]^+$. Similar coordination modes are extremely rare and have only been found in a bis(germylene)-functionalized polyphosphide species.¹⁷ However, in contrast to this bis(Ge)-functionalized polyphosphide, which was formed by thermolysis and could not be isolated in pure form, the present thermolysis reaction is highly selective and quantitative (monitored by $^{31}\text{P}\{^1\text{H}\}$ NMR) and the Si/Ga-polyphosphide species **3** could be isolated in a pure form. In the $^{29}\text{Si}\{^1\text{H}\}$ NMR spectrum of **3**, the signal was observed at 63.4 ppm, slightly downfield-shifted compared to the signal of **2** (57.1 ppm).

The three isomeric mixed metallic Ga/Si/Fe polyphosphides **1–3** are unique compounds and the findings highlight the role of the additional Lewis-acidic Ga center in the transformation pathway, as the reactions which were observed did not resemble those with classical NHSi and NHC.^{15,23} Having ascertained the reaction pathway between pentaphosphaferrrocene and the gallasilylene, the question came up whether similar reactivity can be observed for the pentaarsaferrocene as well.²⁴ Compared to the redox chemistry with its lighter phosphorus analog, the chemistry of $[\text{Cp}^*\text{Fe}(\eta^5\text{-As}_5)]$ is still in its infancy and the reduction is known to be less selective. Often, a mixture of arsenic-rich products is formed. For example, while the reduction of $[\text{Cp}^*\text{Fe}(\eta^5\text{-P}_5)]$ with KH gave selectively the dipotassium salt,²⁵ the reaction with $[\text{Cp}^*\text{Fe}(\eta^5\text{-As}_5)]$ led to the unselective formation of a mixture of arsenic rich species.²⁶ Keeping this in mind, the reaction between $[\text{L}^{\text{Ph}}\text{Si}-\text{Ga}(\text{Cl})\text{L}^{\text{BDI}}]$ and $[\text{Cp}^*\text{Fe}(\eta^5\text{-As}_5)]$ was monitored by ^1H NMR spectroscopy. Interestingly, already after a few minutes reaction time, the reaction is complete, a single reaction product **4** is selectively formed and no intermediate could be detected (Scheme 3). After recrystallization from *n*-hexane, the product **4** forms red prisms in 49% yield which were analyzed by single crystal X-ray diffraction analysis to determine the solid-state structure.

The molecular structure depicted in Fig. 4 shows that a ring expansion occurred to give a novel six-membered silapentaarsa-ring. Interestingly, it should be pointed out that the insertion and ring-expansion reaction behaves differently compared to that with $[\text{Cp}^*\text{Fe}(\eta^5\text{-P}_5)]$ as the gallarylene moiety $[\text{L}^{\text{BDI}}\text{Ga}]$ is not coordinated to the same pnictogen atom as the silicon atom. In the As_5Si fragment, the As4 (As1–As2–As3–As4) unit is nearly planar with the atoms As5 and Si deviating out of the plane. The

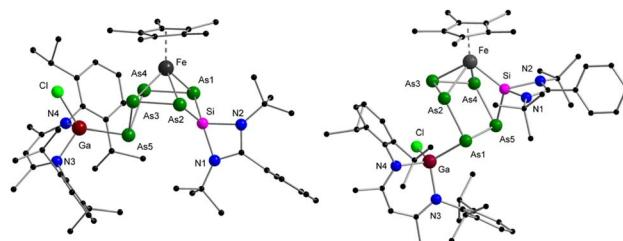
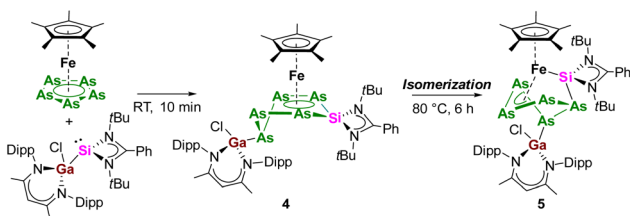


Fig. 4 Molecular structures of complexes **4** (left) and **5** (right) in the solid state. Selected bond distances [Å] and angles [°] in **4**: Si–As1 2.2787(10), Si–As2 2.2985(9), As1–As4 2.3764(5), As2–As3 2.3623(5), As3–As5 2.4563(4), As4–As5 2.4641(5), Ga–As5 2.4046(5); As1–Si–As2 105.00(4), Si–As1–As4 102.03(3), Si–As2–As3 105.34(3), As2–As3–As5 103.27(2), As1–As4–As5 107.12(2), As3–As5–As4 74.030(14). In **5**: As1–As2 2.4467(4), As2–As3 2.3669(5), As3–As4 2.3222(5), As4–As5 2.5375(5), As1–As5 2.3986(4), Ga1–As1 2.4080(4), Si–As5 2.3711(8); As1–As2–As3 103.59(2), As2–As3–As4 97.33(2), As3–As4–As5 107.00(2), As1–As5–As4 103.31(2), As2–As1–As5 99.135(15).

six-membered SiAs_5 -ring shows two shorter As–As bonds (As1–As4 2.3764(4) Å, As2–As3 2.3623(5) Å) and two longer As–As bonds (As3–As5 2.4565(4) Å, As4–As5 2.4641(5) Å), all of which are in the range of As–As single bonds.¹⁸ The Si–As bond lengths of 2.2783(9) Å (Si–As1) and 2.2985(9) Å (Si–As2) are in-between Si–As single (2.359 Å) and double bonds (2.168 Å).^{18,27} In the $^{29}\text{Si}\{^1\text{H}\}$ NMR spectrum, a single signal was detected at –4.7 ppm, high-field-shifted as compared with the polyphosphide compound **2** (57.1 ppm). Compound **4** is not stable in solution (C_6D_6) at room temperature. Already within 12 h, traces of several additional signals are formed (see ESI, Fig. S13‡) and the intensity of the new signals increases faster upon heating the NMR tube at 80 °C (Scheme 3).

After 6 h, the thermal decomposition reaction is complete and one major product **5** is formed, which identity could be identified unambiguously by crystallization from *n*-hexane. Single crystal X-ray diffraction analysis revealed that **5** is an iron-arsasilylene complex which is isostructural to complex **3** (Fig. 4). In the reaction, a ring contraction occurred and a five-membered As₅ ring is formed again, accompanied by migration of the Si-fragment. The As–As distances are between 2.322 Å and 2.537 Å and the Fe–Si bond distance of 2.2224(11) Å is only marginally longer than the corresponding bond length in **3**. Upon thermal isomerization and coordination of the silicon nucleus to the iron center, the respective $^{29}\text{Si}\{^1\text{H}\}$ signal is observed at significant lower field (37.1 ppm).

Given the aforementioned reactivity of the polypnictogen precursors towards the gallasilylene, which are highly selective in terms of the ring-expansion reaction and thermal isomerization to form unprecedented Si/Ga functionalized iron-polyphosphides and -polyarsenides, we turned our interest to the reactions with the heavier germylene analogues. Compared to highly reactive silylenes, the divalent Ge species are less prone to be oxidized. Thus previously was reported that the chloro-germylene $[\text{L}^{\text{Ph}}\text{GeCl}]$ did not show any reactivity with $[\text{Cp}^*\text{Fe}(\eta^5\text{-P}_5)]$.¹⁷ To enhance the reactivity of the germylene and to induce cooperative activation and transformation, the gallagermylene $[\text{L}^{\text{Ph}}\text{Ge}-\text{Ga}(\text{Cl})\text{L}^{\text{BDI}}]$ (**6**) was synthesized conveniently



Scheme 3 Reactivity of pentaarsaferrocene $[\text{Cp}^*\text{Fe}(\eta^5\text{-As}_5)]$ towards gallasilylene $[\text{L}^{\text{Ph}}\text{Si}-\text{Ga}(\text{Cl})\text{L}^{\text{BDI}}]$.



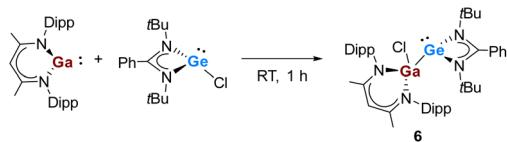
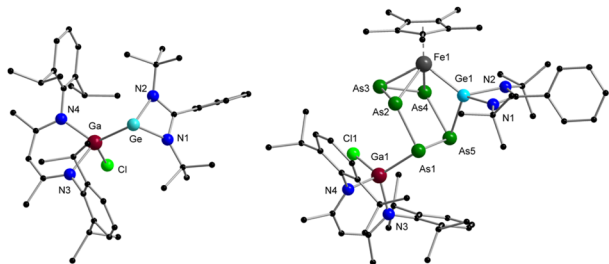
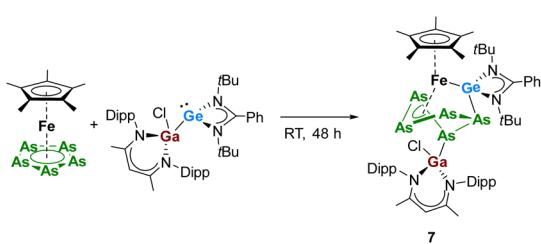
Scheme 4 Synthesis of the gallagermylene $[L^{\text{Ph}}\text{Ge}-\text{Ga}(\text{Cl})L^{\text{BDI}}]$.

Fig. 5 Molecular structures of complexes 6 (left) and 7 (right) in the solid state. Selected bond distances [Å] and angles [°] in 6: Ga–Ge 2.5512(10), Ga–Cl 2.3481(9); Ge–Ga–Cl 120.67(3), N1–Ge–N2 65.33(10), N3–Ga–N4 92.72(10). In 7: As1–As2 2.4345(10), As2–As3 2.3638(12), As3–As4 2.3210(11), As4–As5 2.5510(10), As1–As5 2.4027(10), Ga1–As1 2.4014(9), Ge1–As5 2.4325(9); As1–As2–As3 103.04(4), As2–As3–As4 98.62(4), As3–As4–As5 107.50(4), As1–As5–As4 101.91(3), As2–As1–As5 101.23(3).

from $[L^{\text{Ph}}\text{GeCl}]$ and $[L^{\text{BDI}}\text{Ga}]$ in toluene (Scheme 4). Complex 6 was isolated as yellow crystals in 85% yield and the molecular structure is shown in Fig. 5. The molecular structure resembles that of the silicon analog,^{7a} and the Ga–Ge bond distance is 2.5514(10) Å, similar to that of the recently reported Ga-functionalized germylene comprising an arylsilylamido substituents (2.5533(2) Å).^{7a} Complex 6 results from the oxidative addition reaction of the chloro-germylene towards the Ga(I) species and represents a rare example of a gallagermylene.

In contrast to $[L^{\text{Ph}}\text{Si}-\text{Ga}(\text{Cl})L^{\text{BDI}}]$, the heavier analogue of gallasilylene, $[L^{\text{Ph}}\text{Ge}-\text{Ga}(\text{Cl})L^{\text{BDI}}]$, does not react with $[\text{Cp}^*\text{Fe}(\eta^5\text{-P}_5)]$, even after heating the reaction mixture at 80 °C for 24 h. These findings are in agreement with the lower reactivity of the heavier tetrylenes. In contrast, when equimolar amounts of the arsenic analog $[\text{Cp}^*\text{Fe}(\eta^5\text{-As}_5)]$ were reacted with $[L^{\text{Ph}}\text{Ge}-\text{Ga}(\text{Cl})L^{\text{BDI}}]$ at room temperature, a clean formation of compound 7 (Scheme 5) was observed during the course of two days.

Scheme 5 Reactivity of pentaarsaferrocene $[\text{Cp}^*\text{Fe}(\eta^5\text{-As}_5)]$ towards gallagermylene $[L^{\text{Ph}}\text{Si}-\text{Ge}(\text{Cl})L^{\text{BDI}}]$.

The reaction product 7 was isolated in 53% yield as green crystals. Single crystal X-ray diffraction analysis showed that complex 7 is an iron–germylene complex that is indeed similar to the iron–silylenes 3 and 5. Complex 7 results from cleavage of the Ga–Ge bond and coordination of the $[L^{\text{BDI}}\text{GaCl}]^+$ and $[L^{\text{Ph}}\text{Si}]^+$ fragments towards the Fe-polyarsenide. Complex 7 crystallized in the monoclinic space group $P2_1/c$ with two independent molecules in the asymmetric unit. Therefore, the bonding metrics will be only discussed for one of the molecules. The Fe–Ge bond lengths of 2.2912(11) is slightly longer than that observed in the bis(germylene) functionalized iron-polyphosphide (2.2768(5) Å).¹⁷ The $[\text{Cp}^*\text{Fe}]$ fragment is η^4 -coordinated to the *cyclo*-As₅ unit and in the polyarsenide moiety, the As–As bond distances are between 2.323 Å and 2.551 Å which are typical for polyarsenides.^{14a,26a} The Ga–As bond length (2.4014(9) Å) is comparable to that in the $[L^{\text{BDI}}(\text{Cl})\text{Ga}]$ -functionalized diarsides $[L^{\text{BDI}}\text{Ga}(\text{Cl})\text{As}_2]$ (2.3957(5) Å).²⁸ The ^1H and $^{13}\text{C}[^1\text{H}]$ NMR spectra of 7 show good similarities of the β -diketiminate and amidinate ligand signals as for the thermolysis species 3 and 5, which hinted the formation of a similar product already at room temperature. Interestingly, the reaction leading to the iron-germylene species 7 already proceeds smoothly at room temperature without identifiable intermediates, whereas for silylenes, the reactions leading to the iron-silylenes 3 and 5 requires higher temperatures and different unstable intermediates could be identified and isolated.

To rationalize the observed behavior, DFT calculations (Gaussian16,²⁹ PBE0,³⁰ def2-SVP,³¹ GD3³²) regarding the mechanism of the rearrangement reaction in the gallasilylene/pentaphosphaferrrocene system were initiated with model compounds with cyclopentadienyl (C_5H_5^-) instead of penta-methylcyclopentadienyl (C_5Me_5^-) and only methyl substituents on all heteroatoms (Fig. 6). The calculations provide comprehensive explanations of the observed reactivity. In case of the reaction of $[\text{CpFe}(\eta^5\text{-P}_5)]$ with the gallasilylene (data in black), the sequence starts with a nucleophilic attack of the silylene on one P atom of the P₅ cycle. This leads to the first intermediate **Int1** which has two pathways with moderate activation barriers (>92 kJ mol⁻¹), sufficient to allow its isolation at low temperature. Upon warming to room temperature, the reaction cascade proceeds forward (**Int2–6**). The highest barrier within this cascade amounts to 92.2 kJ mol⁻¹. The initial step of the molecular rearrangement is a gallyl shift from Si to P, followed by silylene migration from the gallyl-P across the P₅ scaffold. Subsequently, the silylene shifts towards the gallyl-P but then inserts into a P–P(Ga) bond to reach an intermediate (**Int7**) that is considerably more stable than the initial one-bond-intermediate (**Int1**) which could also be isolated. The highest activation barrier of 159.3 kJ mol⁻¹ is encountered in the subsequent coordination of Si to Fe. Heating the sample to 80 °C allowed to overcome this computed activation barrier, and lead to a P₄Si moiety coordinated to Fe, but from this intermediate (**Int8**) there is a smaller activation barrier that leads to the thermodynamic minimum species, **Product^M**. Thus, all intermediates whose isolation is apparently feasible were achieved for this reaction.

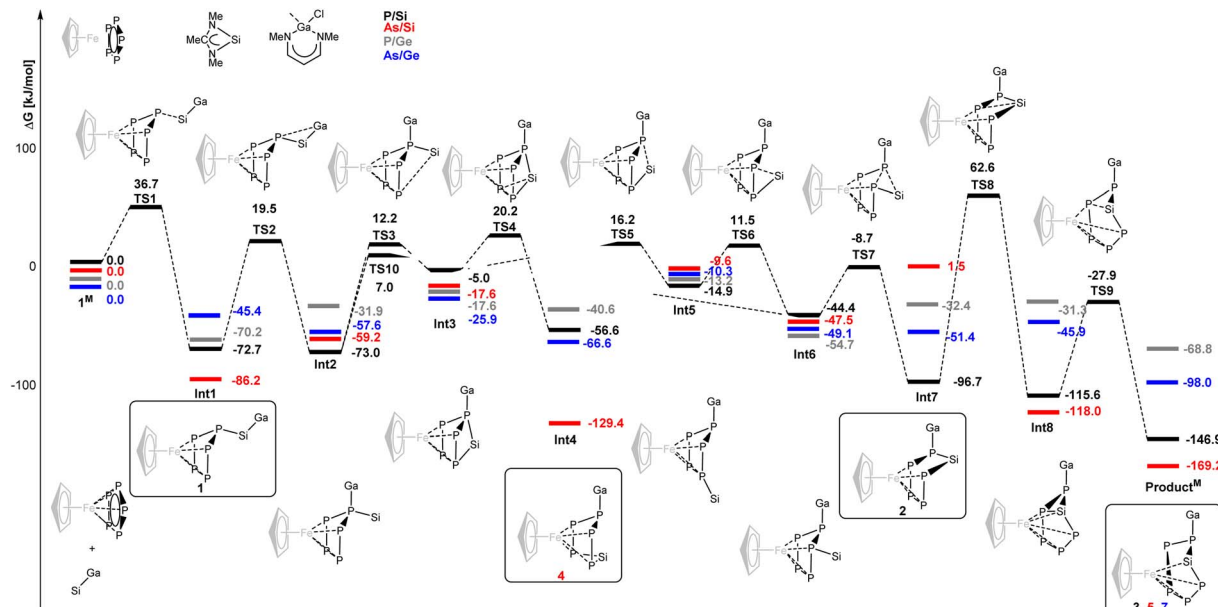


Fig. 6 Computed reaction pathway for model compounds with methyl substituents on N (black: $[\text{CpFe}(\eta^5\text{-P}_5)]$ + arsasilylene, red: $[\text{CpFe}(\eta^5\text{-As}_5)]$ + gallasilylene, grey: $[\text{CpFe}(\eta^5\text{-P})]$ + gallagermylene, blue: $[\text{CpFe}(\eta^5\text{-As}_5)]$ + gallagermylene). Transition states are given for P_5/Si . The highlighted intermediates/products were isolated and the corresponding complex numbers are indicated in the boxes. TS10^M connects Int2 and Int6 .

Interestingly, for the analogous reaction of $[\text{CpFe}(\eta^5\text{-As}_5)]$ with the gallasilylene (data in red), **Int4** is more stable than **Int1** and **Int7**, hence this isomer is dominating the cascade from **Int1** to **Int7**. A thermally induced rearrangement is still possible and leads to **Product^M**. When the reaction between $[\text{CpFe}(\eta^5\text{-P}_5)]$ and the gallagermylene was experimentally investigated (data in grey), no reaction could be observed. Thus, the nucleophilicity of the germylene is insufficient for the activation of the P_5 cycle. This is also reflected in the calculated thermodynamic parameters of the reaction, which show **Int1** as global minimum species.

In contrast, $[\text{CpFe}(\eta^5\text{-As}_5)]$ reacts with the gallagermylene (data in blue). This is in line with a shallower potential energy pathway. The reaction cascade smoothly proceeds and **Product^M** is observed as sole product without isolated intermediates. Two features of the gallatetrylenes are likely to contribute to the distinctly different behavior of these silylenes and germylenes towards pentaphospho- and pentaarsaferrocene compared to previously employed ambiphiles (silylenes, aluminyles). The bond between gallium and another electropositive element (Si, Ge) is rather weak and is cleaved in favor of a Ga-P bond early in the cascade and stays in place for the remainder of the reaction sequence.

Consequently, the P_5/As_5 scaffold is more polarized than in reactions with monofunctional tetrylenes. At the same time, the Ga atom bears a bulky β -diketiminato substituent which prevents the attack of another tetrylene and thus, the reaction stays in strict 1 : 1 stoichiometry.

Conclusions

In summary, we present a full account/study of sequential polypyridogenide transformations of the sandwich compounds

$[\text{Cp}^*\text{Fe}(\eta^5\text{-E}_5)]$ ($\text{E} = \text{P, As}$) by gallatetrylenes. Using the Ga-functionalized silylene, different isomers could be identified, which were formed by nucleophilic attack, ring expansion and ring construction reactions. However, when the respective germylene was employed, no intermediate was observed and only an iron-germylene complex was isolated. In the respective transformations the reaction mechanism was deduced by the isolation and characterization of different isomers. The results showcase the importance of main group element–element cooperativity in polypyridogenide chemistry and indicate future possibilities to discover novel structure motifs, which are difficult to access by other routes.

Data availability

All synthetic protocols, spectroscopic data, supplementary figures and tables, data from quantum chemical calculations and detailed crystallographic information can be found in the ESI.‡ Crystallographic data are available *via* the Cambridge Crystallographic Data Centre (CCDC): 2225385–2225391.

Author contributions

XS synthesized and analysed all compounds with support from LZ. XS conducted X-ray experiments. AH performed and analyzed quantum chemical calculations. PWR, SS and MS proposed the idea, supervised the work, and interpreted the results. All authors contributed to the preparation of the manuscript.

Conflicts of interest

There are no conflicts to declare.

Acknowledgements

The authors are grateful to the Deutsche Forschungsgemeinschaft (DFG) (470309834 RO 2008/21-1 and Sche 384/45-1 and SCHU 1069/26-1). We acknowledge support by the state of Baden-Württemberg through bwHPC and DFG through grant no. INST40/467-1FUGG (JUSTUS cluster).

References

- (a) J. M. Gil-Negrete and E. Hevia, *Chem. Sci.*, 2021, **12**, 1982–1992; (b) J. A. Chipman and J. F. Berry, *Chem. Rev.*, 2020, **120**, 2409–2447.
- (a) J. Park and S. Hong, *Chem. Soc. Rev.*, 2012, **41**, 6931–6943; (b) S. Sinhababu, Y. Lakliang and N. P. Mankad, *Dalton Trans.*, 2022, **51**, 6129–6147; (c) K. Liao, T. C. Pickel, V. Boyarskikh, J. Baesa, D. G. Musaev and H. M. L. Davies, *Nature*, 2017, **551**, 609–613; (d) K. P. Kornecki, J. F. Briones, V. Boyarskikh, F. Fullilove, J. Autschbach, K. E. Schrote, K. M. Lancaster, H. M. L. Davies and J. F. Berry, *Science*, 2013, **342**, 351–354; (e) M. Carrasco, N. Curado, C. Maya, R. Peloso, A. Rodriguez, E. Ruiz, S. Alvarez and E. Carmona, *Angew. Chem., Int. Ed.*, 2013, **52**, 3227–3231; (f) P. D. Dutschke, S. Bente, C. G. Daniliuc, J. Kinas, A. Hepp and F. E. Hahn, *Dalton Trans.*, 2020, **49**, 14388–14392; (g) W. Wang, L. Zhao, H. Lv, G. Zhang, C. Xia, F. E. Hahn and F. Li, *Angew. Chem., Int. Ed.*, 2016, **55**, 7665–7670.
- (a) C. M. Mömming, E. Otten, G. Kehr, R. Fröhlich, S. Grimme, D. W. Stephan and G. Erker, *Angew. Chem., Int. Ed.*, 2009, **48**, 6643–6646; (b) D. W. Stephan and G. Erker, *Angew. Chem., Int. Ed.*, 2010, **49**, 46–76; (c) D. W. Stephan, *Science*, 2016, **354**, aaf7229.
- S. D. Robertson, M. Uzelac and R. E. Mulvey, *Chem. Rev.*, 2019, **119**, 8332–8405.
- (a) Y. Wang, M. Karni, S. Yao, A. Kaushansky, Y. Apeloig and M. Driess, *J. Am. Chem. Soc.*, 2019, **141**, 12916–12927; (b) Y. Xiong, S. Yao, T. Szilvási, A. Ruzicka and M. Driess, *Chem. Commun.*, 2020, **56**, 747–750; (c) X. Chen, H. Wang, S. Du, M. Driess and Z. Mo, *Angew. Chem., Int. Ed.*, 2021, **61**, e2021145; (d) M.-P. Luecke, L. Giarrana, A. Kostenko, T. Gensch, S. Yao and M. Driess, *Angew. Chem., Int. Ed.*, 2021, **61**, e202110398.
- (a) S. P. Green, C. Jones and A. Stasch, *Science*, 2007, **318**, 1754–1757; (b) D. D. L. Jones, I. Douair, L. Maron and C. Jones, *Angew. Chem., Int. Ed.*, 2021, **60**, 7087–7092.
- (a) J. Schoening, A. Gehlhaar, C. Wölper and S. Schulz, *Chem.-Eur. J.*, 2022, **28**, e202201031; (b) A. Bücker, C. Wölper, G. Haberhauer and S. Schulz, *Chem. Commun.*, 2022, **58**, 9758–9761; (c) J. Schoening, C. Wölper and S. Schulz, *Eur. J. Inorg. Chem.*, 2022, e202200638.
- (a) X. Sun, A. Hinz and P. W. Roesky, *CCS Chem.*, 2022, **4**, 1843–1849; (b) Y. Xiong, S. Yao, M. Brym and M. Driess, *Angew. Chem., Int. Ed.*, 2007, **46**, 4511–4513; (c) S. S. Sen, S. Khan, H. W. Roesky, D. Kratzert, K. Meindl, J. Henn, D. Stalke, J.-P. Demers and A. Lange, *Angew. Chem., Int. Ed.*, 2011, **50**, 2322–2325; (d) S. Khan, R. Michel, S. S. Sen, H. W. Roesky and D. Stalke, *Angew. Chem., Int. Ed.*, 2011, **50**, 11786–11789; (e) Y. Wang, T. Szilvási, S. Yao and M. Driess, *Nat. Chem.*, 2020, **12**, 801–807.
- (a) O. J. Scherer and T. Brück, *Angew. Chem., Int. Ed. Engl.*, 1987, **26**, 59; (b) S. Reichl, E. Mädl, F. Riedlberger, M. Piesch, G. Balázs, M. Seidl and M. Scheer, *Nat. Commun.*, 2021, **12**, 5774.
- (a) M. Haimerl, M. Piesch, G. Balázs, P. Mastrorilli, W. Kremer and M. Scheer, *Inorg. Chem.*, 2021, **60**, 5840–5850; (b) H. Brake, E. Peresypkina, A. V. Virovets, W. Kremer, C. Klimas, C. Schwarzmaier and M. Scheer, *Inorg. Chem.*, 2021, **60**, 6027–6039.
- (a) J. Bai, A. V. Virovets and M. Scheer, *Science*, 2003, **300**, 781–783; (b) M. Scheer, A. Schindler, J. Bai, B. P. Johnson, R. Merkle, R. Winter, A. V. Virovets, E. V. Peresypkina, V. A. Blatov, M. Sierka and H. Eckert, *Chem.-Eur. J.*, 2010, **16**, 2092–2107; (c) C. Heindl, E. V. Peresypkina, A. V. Virovets, W. Kremer and M. Scheer, *J. Am. Chem. Soc.*, 2015, **137**, 10938–10941; (d) F. Dielmann, C. Heindl, F. Hastreiter, E. V. Peresypkina, A. V. Virovets, R. M. Gschwind and M. Scheer, *Angew. Chem., Int. Ed.*, 2014, **53**, 13605–13608; (e) R. Yadav, M. Weber, A. K. Singh, L. Münzfeld, J. Gramüller, R. M. Gschwind, M. Scheer and P. W. Roesky, *Chem.-Eur. J.*, 2021, **27**, 14128–14137.
- M. Piesch, F. Dielmann, S. Reichl and M. Scheer, *Chem.-Eur. J.*, 2020, **26**, 1518–1524.
- (a) T. Li, M. T. Gamer, M. Scheer, S. N. Konchenko and P. W. Roesky, *Chem. Commun.*, 2013, **49**, 2183–2185; (b) N. Reinfandt, N. Michenfelder, C. Schoo, R. Yadav, S. Reichl, S. N. Konchenko, A. N. Unterreiner, M. Scheer and P. W. Roesky, *Chem.-Eur. J.*, 2021, **27**, 7862–7871; (c) T. Li, J. Wiecko, N. A. Pushkarevsky, M. T. Gamer, R. Köppe, S. N. Konchenko, M. Scheer and P. W. Roesky, *Angew. Chem., Int. Ed.*, 2011, **50**, 9491–9495.
- (a) X. Sun, A. K. Singh, R. Yadav, D. Jin, M. Haimerl, M. Scheer and P. W. Roesky, *Chem. Commun.*, 2022, **58**, 673–676; (b) C. Riesinger, G. Balázs, M. Seidl and M. Scheer, *Chem. Sci.*, 2021, **12**, 13037–13044.
- R. Yadav, T. Simler, S. Reichl, B. Goswami, C. Schoo, R. Köppe, M. Scheer and P. W. Roesky, *J. Am. Chem. Soc.*, 2020, **142**, 1190–1195.
- R. Yadav, T. Simler, B. Goswami, C. Schoo, R. Köppe, S. Dey and P. W. Roesky, *Angew. Chem., Int. Ed.*, 2020, **132**, 9530–9534.
- R. Yadav, B. Goswami, T. Simler, C. Schoo, S. Reichl, M. Scheer and P. W. Roesky, *Chem. Commun.*, 2020, **56**, 10207–10210.
- P. Pykkö and M. Atsumi, *Chem.-Eur. J.*, 2009, **15**, 12770–12779.
- N. Burford, P. J. Ragogna, K. N. Robertson, T. S. Cameron, N. J. Hardman and P. P. Power, *J. Am. Chem. Soc.*, 2002, **124**, 382–383.
- M. K. Sharma, C. Wölper, G. Haberhauer and S. Schulz, *Angew. Chem., Int. Ed.*, 2021, **60**, 6784–6790.
- C. Riesinger, G. Balázs, M. Bodensteiner and M. Scheer, *Angew. Chem., Int. Ed.*, 2020, **59**, 23879–23884.
- P. Budzelaar, *gNMR for Windows (5.0. 6.0) NMR Simulation Program*, Ivory Soft, Letchworth, U.K, 2006.



23 F. Riedlberger, S. Todisco, P. Mastrorilli, A. Y. Timoshkin, M. Seidl and M. Scheer, *Chem.-Eur. J.*, 2020, **26**, 16251–16255.

24 O. J. Scherer, C. Blath and G. Wolmershäuser, *J. Organomet. Chem.*, 1990, **387**, C21–C24.

25 M. V. Butovskiy, G. Balázs, M. Bodensteiner, E. V. Peresypkina, A. V. Virovets, J. Sutter and M. Scheer, *Angew. Chem., Int. Ed.*, 2013, **52**, 2972–2976.

26 (a) M. Schmidt, D. Konieczny, E. V. Peresypkina, A. V. Virovets, G. Balázs, M. Bodensteiner, F. Riedlberger, H. Krauss and M. Scheer, *Angew. Chem., Int. Ed.*, 2017, **56**, 7307–7311; (b) N. Arleth, M. T. Gamer, R. Köppe, S. N. Konchenko, M. Fleischmann, M. Scheer and P. W. Roesky, *Angew. Chem., Int. Ed.*, 2016, **55**, 1557–1560.

27 M. Driess and R. Janoschek, *J. Mol. Struct.*, 1994, **313**, 129–139.

28 L. Tuscher, C. Helling, C. Wölper, W. Frank, A. S. Nizovtsev and S. Schulz, *Chem.-Eur. J.*, 2018, **24**, 3241–3250.

29 M. J. Frisch, G. W. Trucks, H. B. Schlegel, G. E. Scuseria, M. A. Robb, J. R. Cheeseman, G. Scalmani, V. Barone, G. A. Petersson, H. Nakatsuji, et al, *Gaussian 16, Revision B.01*, Gaussian, Inc., Wallingford, CT, 2016.

30 C. Adamo and V. Barone, *J. Chem. Phys.*, 1999, **110**, 6158–6170.

31 F. Weigend and R. Ahlrichs, *Phys. Chem. Chem. Phys.*, 2005, **7**, 3297–3305.

32 S. Grimme, J. Antony, S. Ehrlich and H. Krieg, *J. Chem. Phys.*, 2010, **132**, 154104.

